Magneto-optical waveguides with polarization independent nonreciprocal phase shift

O. Zhuromskyy, H. Dötsch, M. Lohmeyer, L. Wilkens, P. Hertel
Department of Physics, University of Osnabrück, Germany

Abstract

Magneto–optical waveguides having nonreciprocal phase shift for both TE and TM modes can be prepared by properly adjusting the spatial variation of the Faraday rotation. Such waveguides are attractive to realize optical isolators. We investigate four concepts of magneto–optical waveguides which yield equal nonreciprocal phase shifts for the fundamental TE and TM modes. A polarization independent Mach-Zehnder type integrated optical isolator is presented. All the calculations are performed using material parameters typical for garnet films.

I. Introduction

Reflection of light is an inevitable effect in optical systems. Lasers must be protected from this light, otherwise they become unstable. For this purpose optical isolators are required which rely on the nonreciprocal Faraday rotation of magneto–optical materials. Furthermore, for splitting and combining wavelength multiplexed different routes optical circulators are needed. In the range of optical communication via glass fiber mainly magnetic garnets are available for these nonreciprocal devices. Nowadays only micro–optical isolators and circulators are commercially available. A number of integrated optical isolator and circulator concepts are presented in [1], [2], [3], [4], [5] and [6], [7], respectively. Recently a Mach–Zehnder type integrated optical isolator for TM modes is demonstrated by Fujita et. al. [8]. However, all these devices only employ specific polarizations, TE or TM modes. On the other hand, for practical applications polarization independent isolators and circulators are required. First concepts are presented in [9], [10].

One promising approach to isolators uses Mach–Zehnder interferometers where one or both arms have a nonreciprocal phase shift. In this paper we investigate four different magneto–optical waveguides which can be adjusted in such a way that the nonreciprocal phase shift is equal for both TE and TM modes. Such waveguides are the basis for polarization independent integrated isolators. The wave matching method [11], [12] is used to calculate the guiding modes of rib waveguides. The magneto-optical effect is treated in the framework of perturbation theory.

II. Nonreciprocal phase shift

In the following analysis light propagation is assumed along the z–direction in monomode optical rib–waveguides. The cross section of the waveguides in the x–y–plane is indicated in the Figures below. The permittivity tensor of magnetized media can be written in the form

$$\hat{\varepsilon} = \begin{pmatrix} n^2 & 0 & 0 \\ 0 & n^2 & 0 \\ 0 & 0 & n^2 \end{pmatrix} + \begin{pmatrix} 0 & i\gamma_z & -i\gamma_y \\ -i\gamma_z & 0 & i\gamma_x \\ i\gamma_y & -i\gamma_x & 0 \end{pmatrix}, \tag{1}$$

where the first term represents the permittivity tensor of the media without magnetization, n is the isotropic refractive index. The second term takes into account the gyrotropic effect. Neglecting optical absorption all numbers n^2 and γ_j in equ.(1) are real. The off–diagonal elements of the permittivity

azhuroms@uos.de
M. Lohmeyer is now with the Department of Mathematical Sciences, University of Twente, Enschede, The Netherlands

tensor are related to the specific Faraday rotation by

$$\gamma_j = \frac{\Theta_{\mathrm{F}}^j n \lambda}{\pi}$$

where $j = \{\mathrm{x}, \mathrm{y}, \mathrm{z}\}$, Θ_{F}^j denotes the Faraday rotation for light propagating in j direction and λ is the vacuum wavelength. To describe the Faraday rotation the vector

$$\vec{\Theta}_{\mathrm{F}} = \begin{pmatrix} \Theta_{\mathrm{F}}^{\mathrm{x}} \\ \Theta_{\mathrm{F}}^{\mathrm{y}} \\ \Theta_{\mathrm{F}}^{\mathrm{z}} \end{pmatrix}$$

is used. The Faraday rotation is determined by the magnetizations $\vec{M}_{\mathrm{a}}$ and $\vec{M}_{\mathrm{d}}$ of the octahedral and tetrahedral sublattices, respectively [13]:

$$\left|\vec{\Theta}_{\mathrm{F}}\right| = A \left|\vec{M}_{\mathrm{a}}\right| + D \left|\vec{M}_{\mathrm{d}}\right| , \tag{2}$$

where A and D are the magneto–optical coefficients, which depend on wavelength and composition. $\vec{M}_{\mathrm{a}}$ and $\vec{M}_{\mathrm{d}}$ are aligned antiparallel to each other. $\vec{\Theta}_{\mathrm{F}}$ is parallel or antiparallel to the net magnetization $\vec{M} = \vec{M}_{\mathrm{a}} + \vec{M}_{\mathrm{d}}$ of the film, depending on the magnitudes of the terms of equ. (2).

The off–diagonal element γ_{y} induces a nonreciprocal phase shift for TM modes but has only negligible effect on TE modes [14]. γ_{x} mainly gives rise to a nonreciprocal phase shift for TE modes [15], [16] and γ_{z} causes TE-TM coupling. Furthermore, γ_{x} and γ_{y} also cause weak TE-TM coupling which will be discussed in section VII.

As $|\gamma| \ll n^2$ the gyrotropic effect is treated in the framework of perturbation theory. The electromagnetic fields of the unperturbed guided modes can be written in the form $\vec{E}(x,y)e^{i(\omega t - \beta z)}$, $\vec{H}(x,y)e^{i(\omega t - \beta z)}$, where ω denotes the angular frequency and β is the mode propagation constant. The shift $\delta\beta$ of the wave number β due to gyrotropy is determined by the expression [17]

$$\delta\beta = \omega\varepsilon_0 \frac{\iint \vec{E}^* \Delta\varepsilon \vec{E} dxdy}{\iint [\vec{E} \times \vec{H}^* + \vec{E}^* \times \vec{H}]_{\mathrm{z}} dxdy} , \tag{3}$$

where $\Delta\varepsilon$ is the part of the permittivity tensor representing gyrotropy. Light propagating in the opposite direction can be modelled by reversing the sign of γ. Thus there is a difference of $2\delta\beta$ between the wavenumbers of forward and backward propagating modes.

The cross section of the waveguide can be divided into rectangles with constant permittivity. Thus, inside the rectangles Maxwell's divergence equation $\vec{\nabla} \cdot \vec{D} = 0$ yields $\vec{\nabla} \cdot \vec{E} = 0$. In the semi–vectorial approximation we assume $E_{\mathrm{x}} = 0$ for TE modes and $H_{\mathrm{x}} = 0$ for TM modes. We will obtain the phase shift for TE modes in media with the magnetization along the x direction

$$\delta\beta_{\mathrm{TE}} = \frac{\omega\varepsilon_0}{\beta_{\mathrm{TE}} N} \iint \gamma_{\mathrm{x}} E_{\mathrm{y}} \partial_{\mathrm{y}} E_{\mathrm{y}} dxdy, \tag{4}$$

and for TM modes in media with the magnetization along the y direction

$$\delta\beta_{\mathrm{TM}} = -\frac{\beta_{\mathrm{TM}}}{\omega\varepsilon_0 N} \iint \frac{\gamma_{\mathrm{y}}}{n^4} H_{\mathrm{y}} \partial_{\mathrm{x}} H_{\mathrm{y}} dxdy, \tag{5}$$

where

$$N = \frac{1}{2} \iint [\vec{E} \times \vec{H}^* + \vec{E}^* \times \vec{H}]_{\mathrm{z}} dxdy.$$

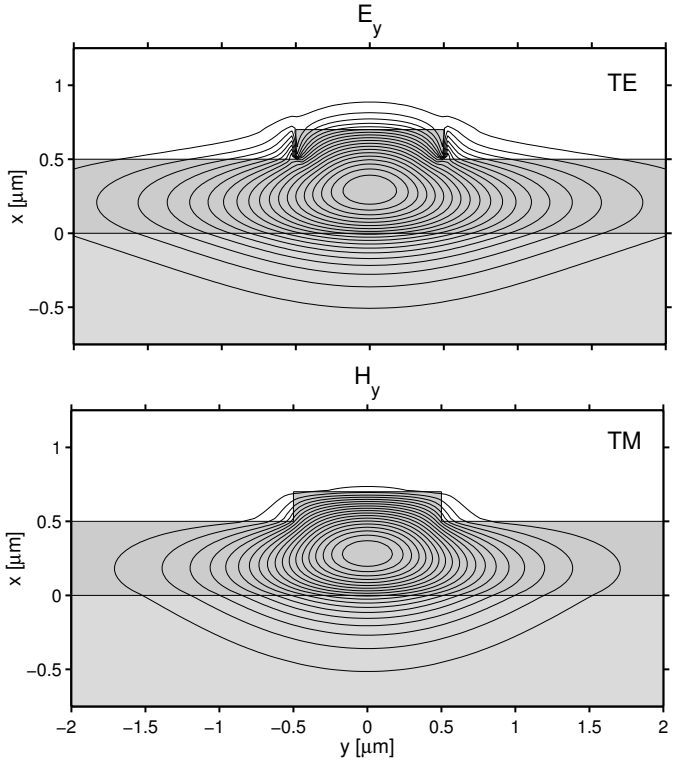

Fig. 1. *Profiles of the dominant field components of the fundamental TE and TM modes in a rib waveguide.*

In the expression for $\delta\beta_{\mathrm{TM}}$ the second order derivatives were neglected. Taking into account the symmetry of the guided TE and TM modes, the largest phase shift will occur in a structure where a boundary separating regions with opposite signs of the Faraday rotation is placed at the maximum of the mode field [14] [15].

The integrals in relations (4,5) can be transformed into integrals of the field intensity along the lines of discontinuities of γ and n: vertical lines for TE modes and horizontal lines for TM modes.

III. Phase shifter with a 90° domain wall

Such a waveguide is sketched in Fig. 2(top). It is divided by a vertical boundary into two regions with magnetization parallel to the x–direction and parallel to the y–direction. The location of the boundary with respect to the waveguide center is denoted by d. The region magnetized along the x axis is responsible for the nonreciprocal phase shift of the TE mode and the in-plane magnetized region causes the nonreciprocal phase shift for the TM mode. The magnitude of the respective nonreciprocal phase shifts depends on the position d of the boundary. A waveguide of this kind can be obtained e. g. by laser annealing [2].

The field profiles of the unperturbed TE and TM modes are shown in Fig. 1. These profiles refer also to all other waveguides discussed below.

Fig. 2(bottom) presents the dependence of the nonreciprocal phase shift on the position of the boundary d. The nonreciprocal phase shift of the TE mode is largest when the domain wall is at the center of the rib. The maximum of the nonreciprocal phase shift of the TM mode is reached when the waveguide is uniformly magnetized along the x axis. The domain wall can be placed such that the nonreciprocal phase shifts of both modes are equal. In this case the nonreciprocal phase shift $\delta\beta$ is approximately $0.8\mathrm{cm}^{-1}$ using the parameters of Table I.

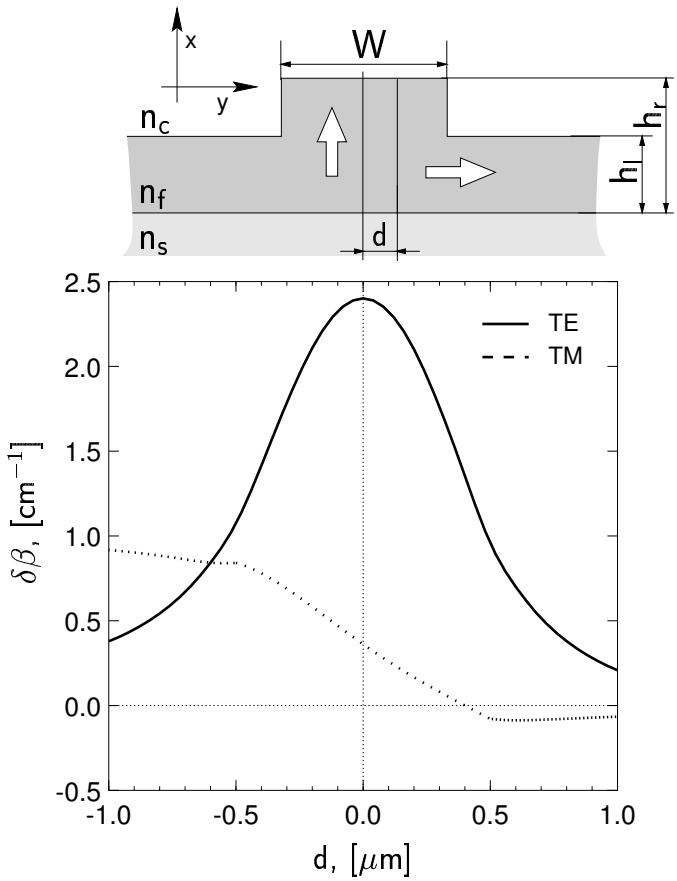

Fig. 2. *Phase shifter with 90° domain wall. The white arrows show the direction of $\vec{\Theta}_F$ in each region. Dependence of the nonreciprocal phase shift of the fundamental TE and TM modes on the position d of the 90° domain wall in the structure described by the parameters given in Table I.*

TABLE I
Waveguide parameters

n_c	1.0	h_r	0.7μm
n_f	2.3	h_l	0.5μm
n_s	1.95	W	1.0μm
λ	1.3μm	Θ_F	1500°/cm

IV. Compensation wall phase shifter with inclined magnetization

We consider a magneto–optical rib wave guide with a 180°–compensation wall [18] and the direction of the magnetization is varied by an external magnetic field, see Fig. 3(top). Thus, the magnetic structure can be adjusted by two parameters: the position d of the wall with respect to the wall center and the inclination angle ϕ. A 180°–compensation wall can be obtained by annealing techniques [18].

The two regions with opposite sign of the Faraday rotation contribute oppositely to the nonreciprocal phase shift of the TM mode. Thus, in this case the nonreciprocal phase shift is induced by the region $(-d, +d)$, the contributions from the outer regions compensate each other. Contrarily the nonreciprocal phase shift of the TE mode from the region $(-d, +d)$ vanishes but the contributions from the outer regions add.

Fig. 3(bottom) presents the dependence of the nonreciprocal phase shifts of the TE and TM modes on the inclination angle ϕ at a constant position d of the compensation wall. Diagrams of this kind

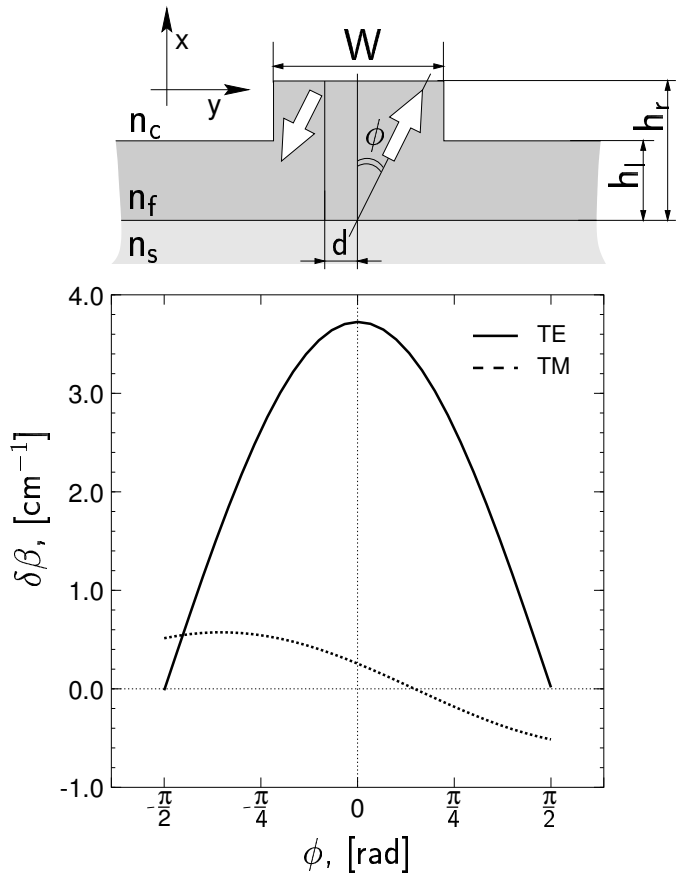

Fig. 3. *Phase shifter with 180°–compensation wall and magnetization inclined by an external magnetic field. The white arrows indicate the direction of $\vec{\Theta}_F$ in each region. The curves show the nonreciprocal phase shift of the fundamental TE and TM modes vs angle ϕ at $d = -0.25\mu m$. The waveguide parameters are presented in Table I.*

show that there are always two special inclination angles: one where the two phase shifts are equal and one where they have opposite sign at equal absolute magnitude.

Fig. 4 a) shows the nonreciprocal phase shift $|\delta\beta|$, equal for both modes, vs position d of the compensation wall. Fig. 4 b) presents the respective inclination angles ϕ. The solid curves refer to the case where the phase shifts are equal, the dotted curves to the case where they have opposite sign at equal absolute magnitude. The largest value of $|\delta\beta|$ is about 0.9cm^{-1}. It is achieved when the wall is located near the rib flanks.

V. Two layer phase shifter

This structure is sketched in Fig.5. It consists of two layers which can be prepared e. g. by subsequent liquid phase epitaxy [14]. The bottom layer is magnetized in–plane. The top layer is magnetized perpendicular to the film plane. It supports a lattice of parallel stripe domains having a period which equals the rib–width [16], Fig. 5 a), or it has a vertical compensation wall at the rib center, Fig. 5 b).

The nonreciprocal phase shifts of the fundamental TE and TM modes are presented in Fig. 5 c) for the two cases depicted in Fig. 5 vs thickness h_b of the bottom layer. The nonreciprocal phase shift $\delta\beta_{TM}$ is the same for the two cases Fig. 5 a) and Fig. 5 b). The Faraday rotation of the bottom layer has been chosen smaller than that of the top layer to adjust $\delta\beta_{TM}$ (see legend of Fig. 5 c). The nonreciprocal phase shift, equal for both TE and TM modes, can reach 3.5cm^{-1} for the compensation wall phase shifter and 2.0cm^{-1} for the phase shifter with domains.

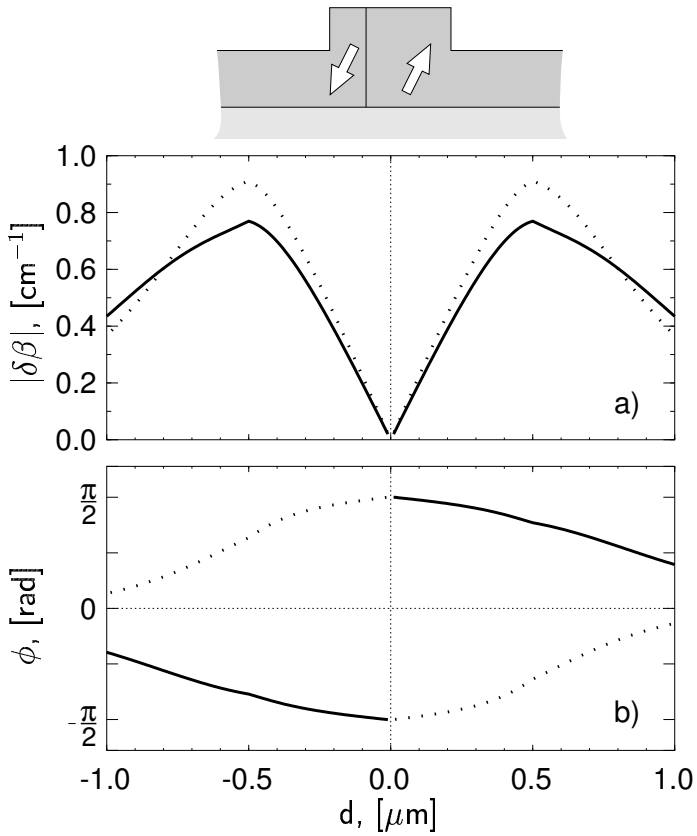

Fig. 4. *The nonreciprocal phase shift $|\delta\beta|$ (a), equal for both TE and TM modes, and the respective inclination angle ϕ (b) vs position of the compensation wall. Solid curves: $\delta\beta_{\rm TE} = \delta\beta_{\rm TM}$, dotted curves: $\delta\beta_{\rm TE} = -\delta\beta_{\rm TM}$. The waveguide parameters are presented in Table I.*

In the case of magnetic domains, Fig. 5 a), all domain walls contribute to $\delta\beta_{\rm TE}$ but with alternating signs. Thus the nonreciprocal phase shift $\delta\beta_{\rm TE}$ is always larger for the single compensation wall at the rib center (Fig. 5 b) then for the domain lattice (Fig. 5 a). For $h_{\rm b} = 0$, the structure of Fig. 5 b) yields a nonreciprocal phase shift $\delta\beta_{\rm TE}$ which is two times larger compared to the structure of Fig. 2 at $d = 0$. This is due to the fact, that the discontinuity of $\gamma_{\rm x}$ is twice as large at the compensation wall in Fig. 5 b) then at the 90° wall Fig. 2.

VI. Asymmetrical waveguide phase shifter

Magneto–optical waveguides, which are symmetrical with respect to the $x-z$ plane and magnetized uniformly along the x axis, produce no nonreciprocal phase shift for TE modes because $\gamma_{\rm x}$ is symmetrical and $E_{\rm y}\partial_{\rm y}E_{\rm y}$ is anti-symmetrical with respect to the $x-z$ plane. Therefore the integral in expression (4) vanishes. The situation changes in an asymmetrical waveguide and we obtain a nonzero nonreciprocal phase shift.

Such a waveguide is shown in Fig. 6(top) while the field profiles of the unperturbed TE and TM modes are shown in Fig. 7. The magnetization is adjusted at an angle ϕ with respect to the x- axis. The nonreciprocal phase shifts for both TE and TM modes are presented in Fig. 6(bottom) as function of the inclination angle ϕ using the parameters listed in Table I.

The nonreciprocal phase shift of the TE mode is quite small compared to that of the TM mode. The reason is that the TE mode is mainly concentrated inside the film near the left vertical waveguide boundary because of the large refractive index difference between film and cover, see Fig. 7. Thus, there is only a small mode amplitude at the boundary where the Faraday rotation changes. Because of the relative small refractive index difference between film and substrate the TM mode penetrates

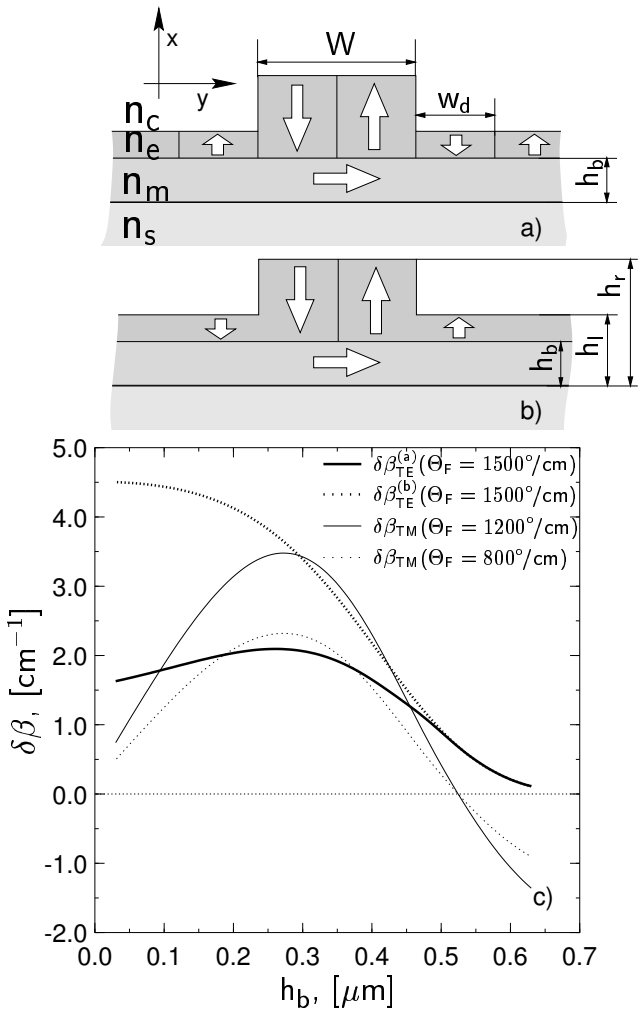

Fig. 5. *Nonreciprocal phase shifters for both TE and TM modes: a) the normally magnetized film supports a lattice of parallel stripe domains; b) a compensation wall is located at the rib center. The white arrows indicate the directions of* $\vec{\Theta}_F$ *in each region. The nonreciprocal phase shift (c) of the fundamental TE and TM mode vs thickness* h_b *of the bottom layer. Waveguide parameters:* $n_s = 1.95, n_m = 2.2, n_e = 2.3, n_c = 1.0, h_r = 0.7\mu m$, $h_l = 0.5\mu m$, $W = 1.0\mu m$, $w_d = 0.5\mu m$, $\lambda = 1.3\mu m$.

deep into the substrate. Therefore, a considerably large effect for the TM mode arises. This different behavior of the modes yields a small nonreciprocal phase shift of about 0.1cm^{-1} equal for both TE and TM modes.

VII. Isolator

A Mach–Zehnder type interferometer with a polarization independent nonreciprocal phase shifter embedded into one of the arms, see Fig. 8, can block the light in one direction while being transparent for light propagating in the opposite direction.

The interferometer arms are adjusted such that a reciprocal phase difference of $\pi/2$ occurs for each mode, TE and TM. The nonreciprocal phase shifter embedded into one of the interferometer arms yields an additional phase shift $-\pi/2$ for the light propagating in forward direction and $+\pi/2$ for the light propagating in the opposite direction. In such a structure the forward propagating light interferes constructively at the end of the interferometer while the backward propagating light interferes destructively.

The phase matching conditions for the interferometer can be written in the form

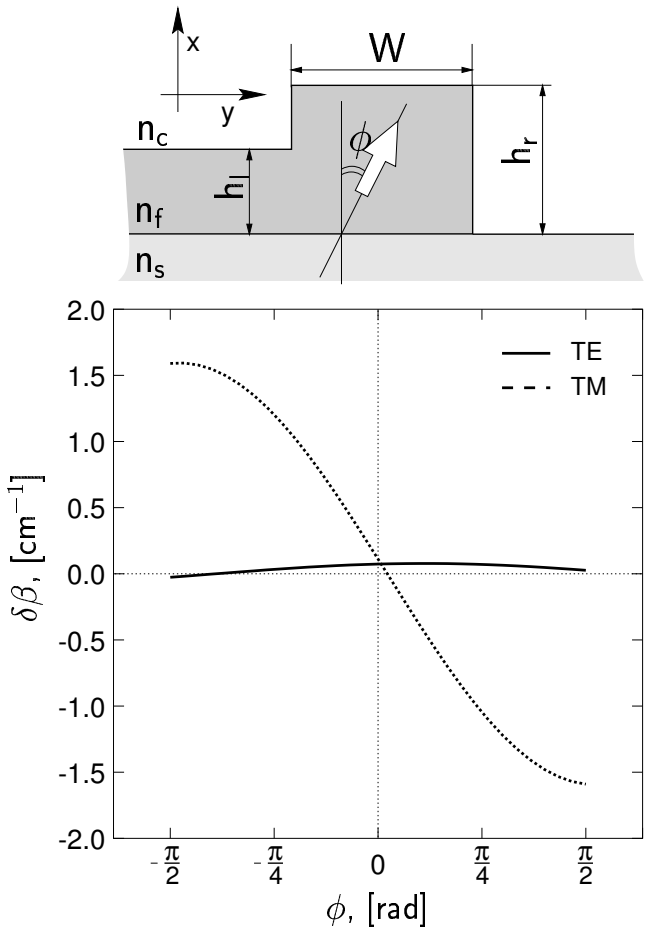

Fig. 6. *Asymmetrical phase shifter with inclined magnetization. The white arrow indicates the direction of* $\vec{\Theta}_{\mathrm{F}}$. *Dependence of the nonreciprocal phase shifts of the asymmetrical waveguide on the angle* ϕ. *The waveguide parameters are given in Table I.*

$$\begin{aligned} \beta_{\mathrm{TE}}(L_1 - L_2) &= \frac{\pi}{2} + \pi n, \\ \beta_{\mathrm{TM}}(L_1 - L_2) &= \frac{\pi}{2} + \pi m, \end{aligned} \tag{6}$$

where β_{TE} and β_{TM} are the wavenumbers of the fundamental modes of the unperturbed waveguide, L_1 and L_2 are the lengths of the two interferometer arms and n, m are integers. The interferometer performance depends on the difference $\Delta L = L_1 - L_2$ of the interferometer arms. System (6) has solutions only when the mode wavenumbers satisfy the condition

$$\frac{\beta_{\mathrm{TE}}}{\beta_{\mathrm{TM}}} = \frac{2n+1}{2m+1}. \tag{7}$$

System (6) yields the difference of the interferometer arms. The entire length of the device depends on the length l of the phase shifter.

The phase matching conditions for the nonreciprocal phase shifters read:

$$\begin{aligned} \delta\beta_{\mathrm{TE}} l &= \frac{\pi}{2} + \pi p, \\ \delta\beta_{\mathrm{TM}} l &= \frac{\pi}{2} + \pi q, \end{aligned} \tag{8}$$

where $\delta\beta_{\mathrm{TE}}$ and $\delta\beta_{\mathrm{TM}}$ are the nonreciprocal phase shifts of the respective modes and p, q are integers.

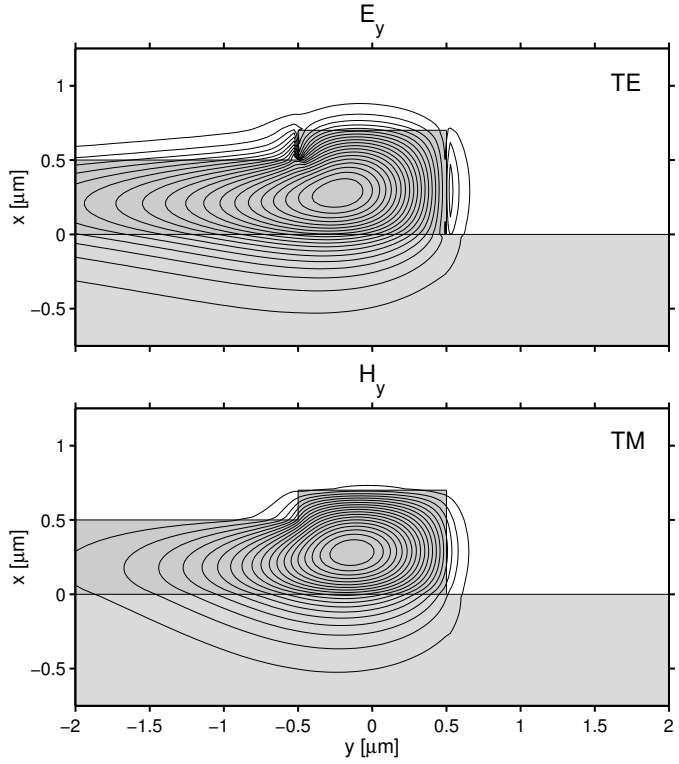

Fig. 7. *Profiles of the dominant field components of the TE and TM modes of the waveguide of Fig. 6 and Table I.*

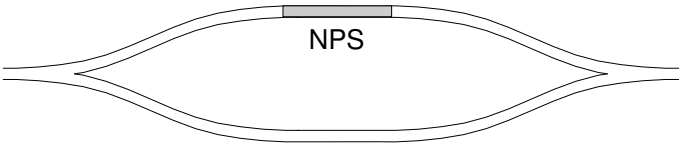

Fig. 8. *Mach–Zehnder type integrated optical interferometer with nonreciprocal phase shifter(NPS) in one of the arms.*

The two layer polarization independent phase shifter (Fig. 5) will be used in the following discussion. Fig. 9 shows the ratio $\beta_{\mathrm{TE}}/\beta_{\mathrm{TM}}$ (top), thickness h_{b} of the bottom layer (center) and the nonreciprocal phase shift $\delta\beta$, equal for both TE and TM mode (bottom), vs total film thickness h_{l} outside the rib. The geometrical parameters are adjusted such that $\delta\beta_{\mathrm{TE}} = \delta\beta_{\mathrm{TM}}$ for $(p = 0, q = 0)$. The solid curves refer to the structure of Fig. 5 a), the dashed curves to Fig. 5 b). The thin horizontal solid and dashed lines of Fig. 9 (top) refer to the numbers (n,m) = (68,67) and (62,61) of expression 6, respectively. The isolator–parameters determined by the thin vertical solid and dashed lines are listed in Table II.

For the discussed waveguide structures the component γ_{z} is zero, which would otherwise cause a strong TE-TM mode conversion. However, the other non-diagonal elements γ_{x} and γ_{y} may cause a weak mode coupling with a coupling coefficient

$$\kappa = \omega\varepsilon_0 \frac{\iint \vec{E}^{*\mathrm{TE}} \Delta\varepsilon \vec{E}^{\mathrm{TM}} dxdy}{\iint [\vec{E}^{\mathrm{TE}} \times \vec{H}^{*\mathrm{TE}} + \vec{E}^{*\mathrm{TE}} \times \vec{H}^{\mathrm{TE}}]_{\mathrm{z}} dxdy}.$$

For the present waveguide structures, κ is in the range of $10^{-4}\mu\mathrm{m}^{-1}$. The maximum conversion induced by mode coupling is given by $\kappa^2/\left(\kappa^2 + (\Delta\beta/2)^2\right)$, where $\Delta\beta = \beta_{\mathrm{TE}} - \beta_{\mathrm{TM}}$. For a power conversion ratio of 10^{-3} the wavenumber mismatch $\Delta\beta = 0.008\mu\mathrm{m}^{-1}$ is required. However, for the waveguides discussed in this paper $|\Delta\beta|$ is larger than $0.1\mu\mathrm{m}^{-1}$, see Fig. 9 ($\Delta\beta^{(a)} = 0.149\mu\mathrm{m}^{-1}$, $\Delta\beta^{(b)} = 0.165\mu\mathrm{m}^{-1}$). Thus, the TE-TM coupling effect can be neglected.

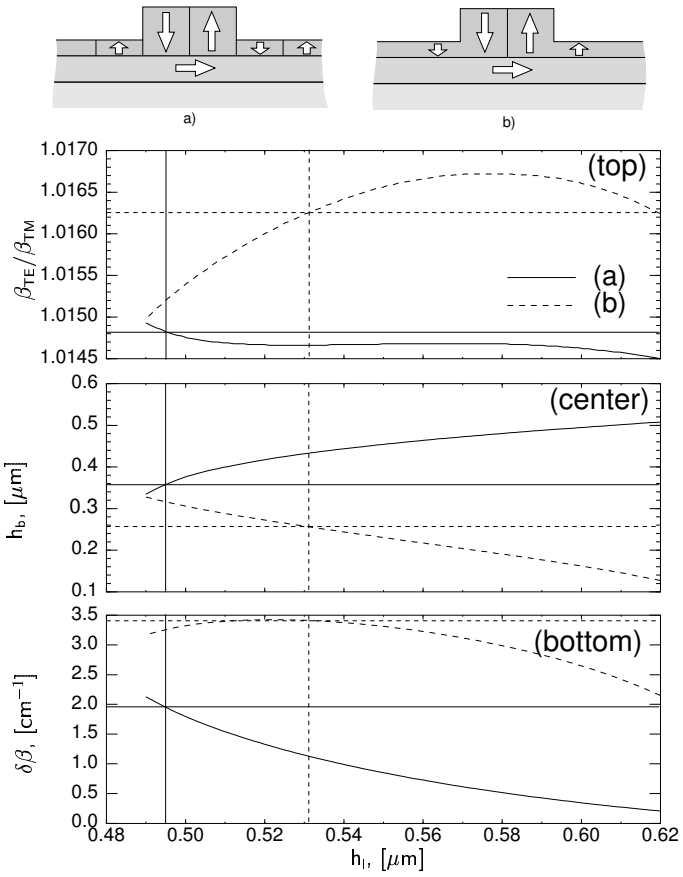

Fig. 9. *The ratio $\beta_{\mathrm{TE}}/\beta_{\mathrm{TM}}$ (top), the thickness h_{b} of the bottom layer (center) and the nonreciprocal phase shift $\delta\beta$ (bottom) vs film thickness h_{l} outside the rib for the waveguides sketched in Fig. 5. The solid curves refer to the structure of Fig. 5a, the dashed curves to the structure of Fig. 5b. The list of parameters is given in Table II.*

VIII. Conclusions

It is demonstrated that magneto–optical waveguides can be designed having a polarization independent nonreciprocal phase shift. Among the four different concepts presented in this paper the most promising structure is the two layer nonreciprocal phase shifter, Fig. 5. For each of the modes the nonreciprocal phase shift is close to the maximum possible value. The concept with a compensation wall (Fig. 5b) allows shorter phase shifters than the domain wall concept, Fig. 5a). However, an additional technological step is required to form the compensation wall at the rib center.

The two concepts of the 90° wall phase shifter, Fig. 2, and of the inclined magnetization compensation wall phase shifter, Fig. 3, have lower performance. The maximum nonreciprocal phase shift in these concepts is about three times smaller compared to the two layer nonreciprocal phase shifter.

For the concept with asymmetrical waveguide, Fig. 6, the nonreciprocal phase shift of the TE mode is very small. However, it can be enhanced considerably by the method presented by Fujita et al [19].

Compared to the concept of polarization independent isolators with two different phase shifters in the interferometer arms [9], the present concept with a polarization independent phase shifter has an advantage: if a nonreciprocal phase shifter is placed in the second arm of the interferometer with the Faraday rotation vector reversed, the entire length of the device can be reduced almost two times. Another reason why the configuration with two polarization independent phase shifters is preferable is that the power loss inside the nonreciprocal phase shifter may differ from that in the rest of the structure. For the non-symmetrical setup it can lead to a reduction of the device performance. This effect can be avoided by using nonreciprocal phase shifters in both interferometer arms [8].

TABLE II

ISOLATOR PARAMETERS

	a	b		a	b
n_c	1.0	1.0	h_b	0.361μm	0.256μm
n_e	2.3	2.3	h_l	0.496μm	0.531μm
n_m	2.2	2.2	w_d	0.5μm	-
n_s	1.95	1.95	W	1.0μm	1.0μm
Θ_F^x	1500°/cm	1500°/cm	$\delta\beta$	1.93cm^{-1}	3.41cm^{-1}
Θ_F^y	800°/cm	1200°/cm	ΔL	21.12μm	19.01μm
h_r	0.7μm	0.7μm	l	8.14mm	4.610mm

REFERENCES

[1] R. Wolfe, J. F. Dillon, R. A. Liberman, and V. J. Fratello, "Broadband magneto-optic waveguide isolator," *Applied Physics Letters*, vol. 57, no. 10, pp. 960–962, 1990.

[2] K. Ando, T. Okoshi, and N. Koshizuka, "Waveguide magneto-optics isolator fabricated by laser annealing," *Applied Physics Letters*, vol. 53, no. 1, pp. 4–6, 1988.

[3] H. Hemme, H. Dötsch, and P. Hertel, "Integrated optical isolator based on nonreciprocal-mode cut-off," *Applied Optics*, vol. 29, no. 18, pp. 2741–2744, 1990.

[4] S. Yamamoto, Y. Okamura, and T. Makimoto, "Analysis and design of semileaky-type thin-film optical waveguide isolator," *IEEE Journal of Quantum Electronics*, vol. 12, no. 12, pp. 764–770, 1976.

[5] T. Shintaku, "Integrated optical isolator based on nonreciprocal higher order mode conversion," *Applied Physics Letters*, vol. 66, no. 21, pp. 2789–2791, 1995.

[6] Y. Okamura, T. Negami, and S. Yamamoto, "Integrated optical isolator and circulator using nonreciprocal phase shifters: a proposal," *Applied Optics*, vol. 23, no. 11, pp. 1886–1889, 1984.

[7] N. Bahlmann, M. Lohmeyer, O. Zhuromskyy, H. Dötsch, and P. Hertel, "Nonreciprocal coupled waveguides for integrated optical isolators and circulators for TM-modes," *Optics Communications*, vol. 161, no. 4-6, pp. 330–337, 1999.

[8] J. Fujita, M. Levy, R. M. Osgood, L. Wilkens, and H. Dötsch, "Waveguide optical isolator based on Mach-Zehnder interferometer," *Applied Physics Letters*, vol. 76, pp. 2158–2160, 2000.

[9] O. Zhuromskyy, M. Lohmeyer, N. Bahlmann, H. Dötsch, and P. Hertel, "Analysis of Polarization Independent Mach-Zehnder Type Integrated Optical Isolator," *Journal of Lightwave Technology*, vol. 17, no. 7, pp. 1200–1205, 1999.

[10] M. Lohmeyer, N. Bahlmann, O. Zhuromskyy, H. Dötsch, and P. Hertel, "Unidirectional magnetooptic polarization converters," *Journal of Lightwave Technology*, vol. 17, no. 12, pp. 2605–2611, 1999.

[11] M. Lohmeyer, "Wave-matching method for mode analysis of dielectric waveguides," *Optical and Quantum Electronics*, vol. 29, pp. 907–922, 1997.

[12] M. Lohmeyer, "Vectorial wave-matching mode analysis of integrated optical waveguides," *Optical and Quantum Electronics*, vol. 30, pp. 385–396, 1998.

[13] P. Hansen, K. Witter, and W. Tolksdorf, "Magnetic and magneto-optical properties of lead- and bismuth-substituted yttrium iron garnet films," *Phys. Rev. B*, vol. 27, pp. 6608–6625, 1983.

[14] M. Wallenhorst, M. Niemöller, H. Dötsch, P. Hertel, R. Gerhardt, and B. Gather, "Enhancement of the nonreciprocal magneto-optic effect of TM modes using iron garnet double layers with opposite Faraday rotation," *Journal of Applied Physics*, vol. 77, no. 7, pp. 2902–2905, 1995.

[15] A. F. Popkov, M. Fehndrich, M. Lohmeyer, and H. Dötsch, "Nonreciprocal TE-mode phase shift by domain walls in magnetooptic rib waveguides," *Applied Physics Letters*, vol. 72, no. 20, pp. 2508–2510, 1998.

[16] M. Fehndrich, A. Josef, L. Wilkens, J. Kleine-Börger, N. Bahlmann, M. Lohmeyer, P. Hertel, and H. Dötsch, "Experimental Investigation of the Nonreciprocal Phase Shift of a TE-Mode in a Magneto-Optic Rib Waveguide," *Applied Physics Letters*, vol. 74, no. 20, pp. 2918–2920, 1999.

[17] G. J. Gabriel and M. E. Brodwin, "The Solution of Guided Waves in Inhomogeneous Anisotropic Media by Perturbation and Variational Methods," *IEEE Transactions on Microwave Theory and Techniques*, vol. MTT-13, pp. 364–370, 1965.

[18] J. P. Krumme and P. Hansen, "New magneto-optic memory concept based on compensation wall domains," *Applied Physics Letters*, vol. 23, no. 10, pp. 576–578, 1973.

[19] J. Fujita, M. Levy, R. M. Osgood, L. Wilkens, and H. Dötsch, "Polarization independent waveguide optical isolator based on nonreciprocal phase shift," 2000, to be published.